Article type: Research letter

The Influence of Anion Size on the Thermoelectric Properties and Seebeck Coefficient Inversion in PDPP-4T

*Augustine O. Yusuf, Kyle N. Baustert, Carter D. Pryor, Kenneth R. Graham**

A. O. Yusuf (Augustine.yusuf@uky.edu), K. N. Baustert (knba253@uky.edu), C.D. Pryor (carter.pryor@uky.edu), Prof. K. R. Graham (Kenneth.graham@uky.edu)

Department of Chemistry, University of Kentucky, Lexington, Kentucky, USA

Keywords:

electrical properties, morphology, semiconducting, thermoelectric, thermoelectricity, organic semiconductor

Abstract

Recent findings show that the Seebeck coefficient (S) can undergo a sign inversion at high doping concentrations in certain π-conjugated polymers. This work investigates how the counterion size influences whether S inversion occurs in electrochemically doped PDPP-4T. The results indicate that at high doping levels, PDPP-4T exhibits S inversion with the small counterion BF_4^-, but not with the large counterion $BArF^-$. Overall, the large $BArF^-$ counterion leads to higher power factors in the most relevant range for thermoelectric devices, whereas the smaller BF_4^- counterion provides the possibility to alter the sign of S by varying the charge-carrier concentration.

Introduction

Fine-tuning the electrical conductivity of conjugated polymers (CPs) through oxidative (p-type) or reductive (n-type) doping plays a crucial role in optimizing the performance of electronic devices and unlocking novel functionalities. These versatile CPs, known for their adjustable electrical and optical properties, ease of fabrication, mechanical flexibility, and biocompatibility, are attractive for widespread applications. For example, they are of interest for solar cells,[1 2] energy storage devices such as batteries and supercapacitors,[3] thermoelectric devices,[4] biosensors,[5] and neuromorphic[6] devices.

The use of doping to regulate the optical, electrical, and thermoelectric properties of organic semiconductors (OSCs) has led to questions on the role of the counterion on the properties under investigation. Here, the counterion, which could either be the dopant ion or an electrolyte ion, interacts with the charge carrier on the OSC and impacts the polymer morphology. While the OSC-counterion interactions are known to influence material properties and device behavior, the complex nature of the doped materials can make it difficult to identify why or how a counterion has a certain impact.[7] In terms of thermoelectric behavior, counterion size has been observed to influence the resulting thermoelectric performance.[8-10] Here, the measure of a thermoelectric material's performance is encapsulated in the figure-of-merit, ZT, which is proportional to the square of the Seebeck coefficient (S^2) multiplied by the electrical conductivity (σ). Optimization of ZT can be difficult, as S and σ are inversely related such that an increase in σ typically results in a decrease in S. Counterions provide one way to adjust this tradeoff.[8, 9, 11]

While several groups have investigated how the counterion can be used to modulate the power factor, it is not known how the counterion size may impact the inversion of the sign of S that has recently been observed to occur with increasing doping levels in conjugated polymers.[12-14] The Seebeck coefficient is influenced by the energy distribution of mobile charge carriers relative to the Fermi energy level (E_F) and their energy dependent mobility. Typically, S is positive in a p-type semiconductor and negative in an n-type semiconductor. However, a change in the sign of S can occur in highly doped polymers.[13-15] This phenomenon provides additional insight into charge transport in CPs and could facilitate the creation of complete thermoelectric modules using p-type and n-type legs made with the same polymer-dopant system, but with varying doping levels. To use this approach to create higher performing materials, it will be important to understand both how the polymer and dopant/counterion chemistry and morphology influence S inversion.

We previously presented a model to explain the origin of the sign change of S.[12] This model relies on delocalized charge carriers in the crystalline regions with a more band-like transport mechanism and localized charge carriers in the amorphous regions with a more hopping-like transport mechanism, with the carriers in the different regions having opposite signs. This model implies that for an inversion of S to occur, both the crystalline and amorphous regions should persist at high doping concentrations. Significant disruption of the crystalline domains is known to occur with larger dopants or counterions, and thus our model would suggest that it is more likely for S inversion to be observed with smaller dopants. Indeed, previous reports of S inversion

in CPs all use small counterions. [12, 14, 16] For example, a sign change in S at high doping levels has been reported using small counterions or dopants, including HCl,[14] $FeCl_3$,[17] and $NOBF_4$,[12] while reports of S inversion remain absent for large dopants such as $Mo(tfd)_3$ and its derivatives,[9] dodecaboranes,[18] or large electrolyte counterions like $BArF^-$.[11]

A recent manuscript by Dyaga, *et al.* showed that S inversion occurs in two different CPs when $FeCl_3$ is used as a dopant, but does not occur when magic blue is used as a dopant.[19] In their work it is shown that $FeCl_3$ penetrates into crystalline domains whereas magic blue does not, highlighting the potential influence of dopant location and morphology. Another interesting finding that hints at the role of morphology compares low and high molecular weight (MW) variants of the same polymer backbone, and observes S inversion from positive to negative in the higher MW polymer and no inversion in the lower MW polymer.[20] In general, this combination of work highlights that polymer morphology and dopant or counterion distribution are important in determining whether an inversion of S occurs.

In this work we investigate how different counterion sizes influence S inversion in Poly[2,5-bis(2-octyldodecyl)pyrrolo[3,4-c]pyrrole-1,4(2H,5H)-dione-3,6-diyl)-alt-(2,2’;5’,2’’;5’’,2’’’-quaterthiophen-5,5’’’-diyl)] (PDPP-4T). We employ tetrafluoroborate (BF_4^-) and tetrakis(3,5-bis(trifluoromethyl)phenyl)borate ($BArF^-$) as electrolyte anions with drastically different sizes and use electrochemical doping to quantify the charge-carrier densities in the films. By combining quantitative charge-carrier densities from electrochemical doping with spectroelectrochemistry, electron paramagnetic resonance, electrical conductivity, and S measurements we present our findings on how the size of the dopant ion affects S inversion in PDPP-4T.

Results and Discussion

The materials used in this work are presented in Figure 1. Here, PDPP-4T is selected due to its pronounced change in S from positive to negative with both $FeCl_3$ and $NOBF_4$ as chemical dopants.[12] The counterions are selected based on their large difference in ionic diameter, where BF_4^- has a diameter of *ca*. 5.6 Å and $BArF^-$ has a diameter of *ca*. 15.4 Å, similar spherical shapes, and literature precedence.[11,21,22,23] While $BArF^-$ contains phenyl groups, no π-π interactions are expected with the polymer backbone due to the high degree of steric hindrance from the neighboring bis(trifluoromethyl)phenyl groups. The patterned polymer films were fabricated by spray coating the polymer ink on ITO substrates and the PDPP-4T was electrochemically doped using chronocoulometry to quantify the charge-carrier density. The quantification of charge-carrier density is important in determining why the Seebeck sign changes, and is difficult for the more commonly used approaches of chemical doping or ion exchange doping.

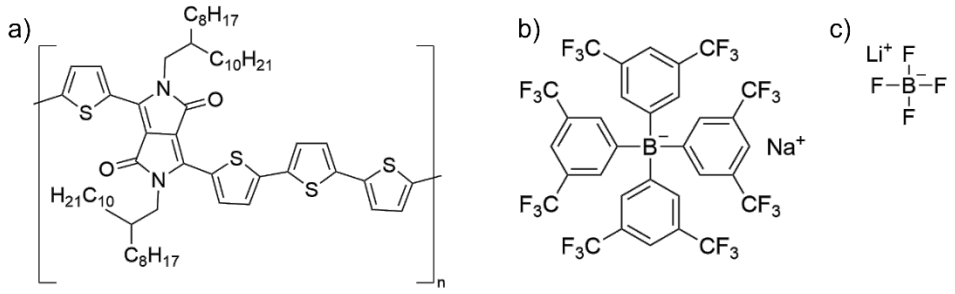

Fig. 1 Chemical structures of a) PDPP-4T, b) NaBArF, and c) $LiBF_4$

Spectroelectrochemistry is used to probe the absorbance of spray-coated PDPP-4T films with BF_4^- and $BArF^-$ at varying charge-carrier concentrations. The spectra in Figure 2a show that at lower charge-carrier densities (between 7.0×10^{19} cm^{-3} and 5.5×10^{20} cm^{-3}), the P1 absorbance peak for PDPP-4T:$BArF^-$ is lower in energy by at least 0.05 eV compared to PDPP-4T:BF_4^-, suggesting more delocalized polarons with $BArF^-$, which is consistent with other works where counterion size is varied. [9, 11, 18] As doping increases, the P1 peak undergoes a hypsochromic shift for $BArF^-$ and a bathochromic shift for BF_4^-, resulting in a difference of only 0.034 eV at a charge-carrier density of 1.1×10^{21} cm^{-3}. Following previous work, we attribute the hypsochromic shift with $BArF^-$ to an inrease in morphological disorder with increasing charge-carrier density, while the bathochromic shift with BF_4^- is suggested to arise from increased polaron delocalization at higher doping concentration.[9, 11] As the charge-carrier density increases beyond *ca.* 2×10^{21} charge-carriers cm^{-3} a significant decrease in the P1 peak intensity is observed. This decrease is accompanied by the emergence of a new peak at 0.87 eV, which indicates a significant change in the electronic structure of the doped materials occurs with both counterions.

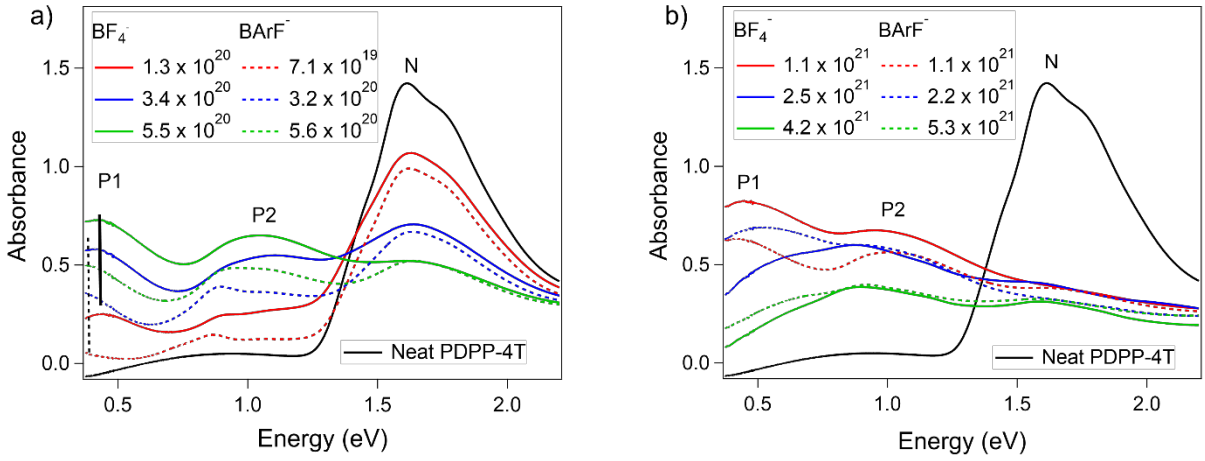

Fig. 2 UV-Vis-NIR absorbance in the a) lower and b) higher doping regimes for PDPP-4T with BF_4^- and $BArF^-$ as counterions

Electron paramagnetic resonance (EPR) spectra were recorded to gain further insight into the nature of the charge carriers, as shown by the integrated EPR signal in Figure S1 (Supplementary Infortmation). Importantly, the EPR measurements only probe unpaired electrons (polarons)

and are not sensitive to spinless charge carriers (e.g., bipolarons), thus they provide insight into the nature of the charge carriers and not the total number of charge carriers. Here, we observe that the EPR signal intensity for PDPP-4T:BArF$^-$ is *ca.* twice that of PDPP-4T:BF_4^- for a given charge-carrier density, which indicates PDPP-4T:BArF$^-$ has more polarons (unpaired spins) while PDPP-4T:BF_4^- forms a higher fraction of bipolarons (no unpaired spins). This observation is consistent with similar counterion size dependencies observed for rr-P3HT and could be attributed to the ability of the BF_4^- counterions to more closely approach each other to favor bipolaron formation.[11] Also consistent with previous results, the EPR data shows that after an initial jump in the concentration of unpaired electrons, additional charge-carriers lead to the formation of bipolarons.[11, 12, 24] This trend is evidenced by the large plateau between 3×10^{20} and 3×10^{21} charge-carriers cm^{-3}. Interestingly, the new absorbance peak at 0.87 eV does correspond with a decrease in the concentration of unpaired electrons.

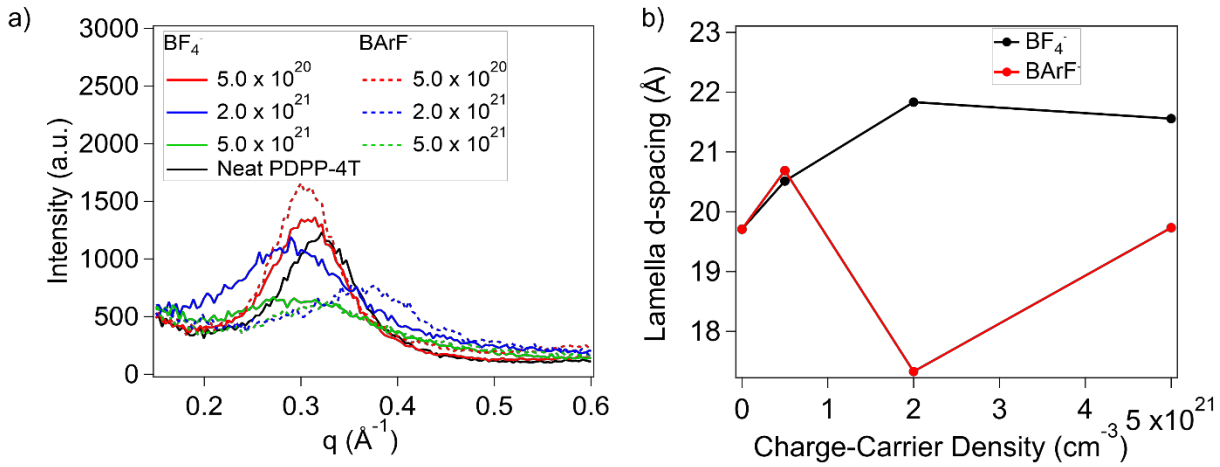

Fig. 3 a) Integrated GISAXS spectra showing changes in peak position and intensity as a function of charge-carrier density and counterion size, and b) GISAXS plot of the calculated d-spacing (100) as a function of charge carrier density

Grazing-incidence wide-angle X-ray scattering (GIWAXS) measurements were recorded to probe the impact of the counterion on the polymer morphology, with the extracted spectra and (100) d-spacings displayed in Figure 3. At low charge-carrier densities of 5×10^{20} charge-carriers cm^{-3}, both BF_4^- and BArF$^-$ show an increase in (100) d-spacing from 19.7 Å for the neat film to 20.5 and 20.7 Å, respectively. As the charge-carrier density is further increased to 2×10^{21} cm^{-3}, the d-spacing further increases for BF_4^-, which suggests that BF_4^- is intercalating between the sidechains. Surprisingly, BArF$^-$ leads to a decrease in d-spacing to only 17.3 Å at 2×10^{21} charge-carriers cm^{-3}, which is less than in the neat film. This shift is consistent with BArF$^-$ being excluded from the crystalline regions at this intermediate concentration,[19] as was observed with magic blue doping in previous work. Furthermore, the decrease in scattering intensity could indicate that the crystalline regions of PDPP-4T where BArF$^-$ initially intercalated become amorphous at higher doping concentrations and only BArF$^-$-free crystalline regions remain intact at higher doping concentrations.

Figure 4a shows S and σ for the PDPP-4T films as a function of charge-carrier density. At low charge-carrier densities both counterions lead to positive S, as expected for p-type doping. However, at high charge-carrier densities (> 4 × 10^{21} cm^{-3}) S is negative with BF_4^-, while it remains positive at all charge-carrier densities with $BArF^-$. Such results support that morphology is important in determining whether S undergoes a sign inversion and further supports that small counterions make it more likely that inversion of S will occur. The use of chronocoulometry to quantify the charge-carrier density allows us to exclude the possibility that different charge-carrier concentrations could be responsible for the counterion effect on S inversion. To further verify that the smaller counterion leads to Seebeck conversion while the larger counterion prevents this inversion, we conducted anion exchange doping. Here, highly doped PDPP-4T films with BF_4^- (6.4 x 10^{21} cm^{-3}) were subject to anion exchange with $BArF^-$. Initially, S with BF_4^- is -110 µV/K and after anion exchange with $BArF^-$ it shifts to +116 µV/K, which further supports that the nature of the anion has a major influence over whether S inversion occurs.

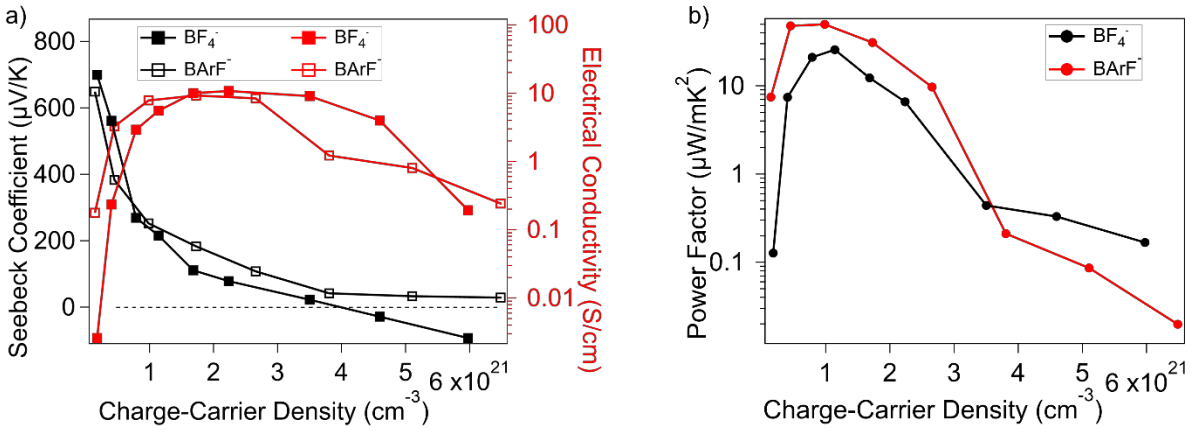

Fig. 4 a) Seebeck coefficient and electrical conductivity, and b) thermoelectric power factor of electrochemically doped PDPP-4T with $BArF^-$ and BF_4^- at varying charge-carrier densities

Outside of the inversion of S, the trends in σ and S agree with previous results on *regioregular*-poly(3-hexylthiophene), P3HT, with BF_4^- or $BArF^-$ as counterions.[11] As with P3HT, $BArF^-$ leads to higher σ and lower S compared with BF_4^- at low charge-carrier densities. Here, the increased σ is attributed to more delocalized charge-carriers owing to the decreased Coulomb interactions afforded by the large $BArF^-$ counterion, while the decreased S is attributed to decreased energetic disorder with $BArF^-$ arising from this same decrease in Coulomb interactions.[11] At higher charge-carrier densities the trends reverse, as Coulomb interactions become negligible[25] and the increased morphological disorder with $BArF^-$ leads to lower σ and larger S. Significantly larger power factors are observed for $BArF^-$ in the most relevant doping regimes for thermoelectrics, which highlights the importance of dopant or counterion selection in the development of organic thermoelectrics.

Conclusion

Our work contributes to the growing understanding of counterion effects in organic thermoelectric materials and the inversion of S. With the inversion of S at high charge-carrier densities for the smaller counterion BF_4^- and not for $BArF^-$, our work supports that smaller counterions are more likely to lead to S inversion. The spectroelectrochemistry data, higher σ, and lower S observed with $BArF^-$ at lower doping concentrations support that larger counterions minimize Coulomb interactions and lead to more delocalized charge carriers. The differences in GISAXS trends with BF_4^- and $BArF^-$ indicate that the counterion has a large impact on morphology, and this difference in morphology likely influences whether the sign of S inverts. Understanding why smaller counterions are more likely to lead to S inversion is a question that we are currently investigating, with current results and models pointing to disruption of crystallinity by large counterions as being an important factor. From an applied perspective, our results further emphasize the importance of the dopant or counterion structure in determining the thermoelectric performance of conjugated polymers.

Material/Methods

Materials

Poly[2,5-bis(2-octyldodecyl)pyrrolo[3,4-c]pyrrole-1,4(2H,5H)-dione-3,6-diyl)-alt-(2,2’;5’,2’’;5’’,2’’’-quaterthiophen-5,5’’’-diyl)] (PDPP-4T), was purchased from Ossila Ltd. Electrolytes lithium tetrafluoroborate ($LiBF_4$) and sodium tetrakis[3,5-(bistrifluoromethyl)phenyl]borate (NaBArF) were purchased from Alfa Aesar. All electrolyte solutions were prepared to 10 mM concentrations in anhydrous acetonitrile from VWR which was dried over molecular sieves and degassed using four freeze-pump-thaw cycles.

Solution and Film Preparation

A 2 mg/mL solution of PDPP-4T in chlorobenzene was prepared and stirred overnight at 60 °C. An equal volume of chloroform was then added to the solution to reduce it to 1 mg/mL. This solution was allowed to stir for another 30 minutes at 30 °C. ITO-coated glass substrates were cleaned sequentially with sodium dodecylsulfate solution, DI water, acetone, and isopropanol for 15 minutes each. After drying the substrates with nitrogen, they were UV-ozone cleaned for 30 minutes. Spray coating was performed with a SimCoat Ultrasonic Spray Coating System (Sonotek, U.S.) using a nozzle-substrate distance of 82 mm, nitrogen pressure of 0.3 psi, generator power of 1.8 W, and an actuation frequency of 120 kHz. The polymer layer was deposited using 10 passes with a liquid infusion rate of 0.1 mL/min.

Spectroelectrochemistry

Spectroelectrochemistry measurements were performed with electrochemical doping of the polymer films for 60 to 180 seconds using chronocoulometry with a VersaStat4 electrochemical analyzer (Princeton Applied Research) to monitor the injected charge. ITO-coated glass substrates (Delta Technologies, 70-100 Ω/□) served as the working electrode, with a silver wire reference electrode and a platinum wire counter electrode. After doping, the films were removed from the

electrolyte solution and allowed to dry. Absorbance was measured on the dried films from 300 to 3300 nm using an Agilent Technologies Cary 5000 UV-vis-NIR spectrophotometer.

EPR

Films for EPR were electrochemically doped in the same manner as those for spectroelectrochemistry. For EPR the ITO-coated glass substrates that were used as the working electrodes were cut into strips roughly 2 mm wide to fit in an EPR tube. EPR measurements were performed using a Bruker EMX Plus x-band instrument operating at a microwave frequency of approximately 9.7 GHz. The data was integrated and corrected using the respective q-values for each measurement.[12]

Grazing-incidence small angle X-ray scattering (GISAXS)

Films fabricated on ITO-coated glass substrates and electrochemically doped using the methods above were used for this purpose. The measurements were conducted using a Xeuss 2.0 system from Xenocs housing a copper anode X-ray source (Cu Kα X-ray, I=1.5418 Å). The stage for the sample was tilted towards the X-ray source by 0.16° and the acquisition time was set at 600s with 2θ ranging between 3.5 and 22°.

Seebeck and Electrical Conductivity

To measure the Seebeck coefficient and electrical conductivity, we used a custom-built device with the sample geometry designed to reduce errors associated with thin film measurements.[26] ITO-coated glass substrates (20 mm × 20 mm) were used as the working electrodes for the Seebeck measurements. Here, thermal evaporation through a shadow mask was used to coat the ITO with C_{60} (40 nm) and bathocuproine (10 nm) in the electrode pattern reported previously.[26] The coated ITO was then etched through suspending the substrates over a freshly prepared aqua regia solution for 8 minutes and the organic protecting layer removed through rinsing with toluene and chloroform. Polymer films were then coated on the ITO-patterned substrates through the ultrasonic spray coating method described earlier, utilizing a shadow mask to define the polymer area. The substrates were further transferred to a thermal evaporator, where 100 nm of bismuth was thermally deposited through a shadow mask at 1×10^{-6} Torr. This bismuth layer served as a reference for monitoring the temperature difference across the substrate during the Seebeck measurements (calibrated S of Bi thin film = -62.1 ± 2.6 μV K^{-1}). As the temperature difference between the ITO contacts increased, the voltages across both the polymer and bismuth films were simultaneously recorded. The PDPP-4T film was electrochemically doped through connecting the two electrode lines for Seebeck measurements to the potentiostat and using these lines as the working electrodes in a three-electrode electrochemical cell. Chronocoulometry was used for doping the PDPP-4T as detailed in the spectroelectrochemistry section. For electrical conductivities, a Keithley multimeter was used to measure the two-probe resistances across the films.

Film Thickness

Film thicknesses were measured with a Dektak 6M/32 profilometer and the final thickness values used were an average of at least three measurements per film.

Anion Exchange

The films were prepared by first doping PDPP-4T films with BF_4^- as the counterion using the initial standard electrochemical procedure mentioned above. After doping, the films were immersed in a 75 mM NaBArF electrolyte solution for 60 seconds. The charge carrier concentration with $BArF^-$ is determined by the initial BF_4^- doping, assuming no dedoping occurred.

Data availability

The data used to support these findings are included within this article and its supplemental material. Raw data is available from the corresponding author, upon reasonable request.

Supporting Material

Supporting Information is available from Springer or from the author.

Acknowledgements

A.O.Y., K.N.B., C.D.P. and K.R.G. acknowledge the National Science Foundation (DMR-2349830) for primary support of this work and the National Science Foundation under cooperative agreement No. 1849213 for the ultrasonic spray coater used in this work. This work was performed in part at the U.K. Center for Electron Microscopy, a member of the National Nanotechnology Coordinated Infrastructure (NNCI), which is supported by the National Science Foundation (NNCI-2025075). A.O.Y. wishes to thank Michael J. Detisch for the training provided while using the Xeuss 2.0 system from Xenocs for GISAXS measurements.

Conflict of Interest Statement

On behalf of all authors, the corresponding author states that there is no conflict of interest.

References

(1) Hyun Suh, E.; Beom Kim, S.; Jung, J.; Jang, J. Extremely Electron-Withdrawing Lewis-Paired CN Groups for Organic p-Dopants. *Angewandte Chemie* **2023**, *135* (37), e202304245. DOI: 10.1002/ange.202304245 (acccessed 2024-04-22 23:51:40).Wiley Online Library.
(2) Zhao, Y.; Wei, J.; Li, H.; Yan, Y.; Zhou, W.; Yu, D.; Zhao, Q. A polymer scaffold for self-healing perovskite solar cells. *Nature communications* **2016**, *7* (1), 10228.

(3) Manjakkal, L.; Pullanchiyodan, A.; Yogeswaran, N.; Hosseini, E. S.; Dahiya, R. A Wearable Supercapacitor Based on Conductive PEDOT:PSS-Coated Cloth and a Sweat Electrolyte. *Advanced Materials* **2020**, *32* (24), 1907254. DOI: https://doi.org/10.1002/adma.201907254.
(4) Ke, Z.; Chaudhary, J.; Flagg, L. Q.; Baustert, K. N.; Yusuf, A. O.; Liu, G.; You, L.; Graham, K. R.; DeLongchamp, D. M.; Mei, J. Controlled Dedoping and Redoping of N-Doped Poly(benzodifurandione) (n-PBDF). *Advanced Functional Materials n/a* (n/a), 2400255. DOI: https://doi.org/10.1002/adfm.202400255.
(5) Menaker, A.; Syritski, V.; Reut, J.; Öpik, A.; Horváth, V.; Gyurcsányi, R. E. Electrosynthesized surface-imprinted conducting polymer microrods for selective protein recognition. *Advanced Materials* **2009**, *21* (22), 2271-2275.
(6) Keene, S. T.; Lubrano, C.; Kazemzadeh, S.; Melianas, A.; Tuchman, Y.; Polino, G.; Scognamiglio, P.; Cinà, L.; Salleo, A.; van de Burgt, Y. A biohybrid synapse with neurotransmitter-mediated plasticity. *Nature Materials* **2020**, *19* (9), 969-973.
(7) Thomas, E. M.; Peterson, K. A.; Balzer, A. H.; Rawlings, D.; Stingelin, N.; Segalman, R. A.; Chabinyc, M. L. Effects of Counter-Ion Size on Delocalization of Carriers and Stability of Doped Semiconducting Polymers. *Advanced Electronic Materials* **2020**, *6* (12), 2000595. DOI: 10.1002/aelm.202000595 (acccessed 2024-04-06 02:18:49).DOI.org (Crossref).
(8) Culebras, M.; Gómez, C. M.; Cantarero, A. Enhanced thermoelectric performance of PEDOT with different counter-ions optimized by chemical reduction. *Journal of Materials Chemistry A* **2014**, *2* (26), 10109-10115, 10.1039/C4TA01012D. DOI: 10.1039/C4TA01012D.
(9) Liang, Z.; Zhang, Y.; Souri, M.; Luo, X.; Alex; Li, R.; Zhang, Y.; Wang, T.; Kim, D.-Y.; Mei, J.; et al. Influence of dopant size and electron affinity on the electrical conductivity and thermoelectric properties of a series of conjugated polymers. *Journal of Materials Chemistry A* **2018**, *6* (34), 16495-16505. DOI: 10.1039/c8ta05922e.
(10) Chen, C.; Jacobs, I. E.; Kang, K.; Lin, Y.; Jellett, C.; Kang, B.; Lee, S. B.; Huang, Y.; BaloochQarai, M.; Ghosh, R.; et al. Observation of Weak Counterion Size Dependence of Thermoelectric Transport in Ion Exchange Doped Conducting Polymers Across a Wide Range of Conductivities. *Advanced Energy Materials* **2023**, *13* (9), 2202797. DOI: 10.1002/aenm.202202797 (acccessed 2024-04-19 13:15:25).Wiley Online Library.
(11) Baustert, K. N.; Bombile, J. H.; Rahman, M. T.; Yusuf, A. O.; Li, R.; Huckaba, A. J.; Risko, C.; Graham, K. R. Combination of Counterion Size and Doping Concentration Determine the Electronic and Thermoelectric Properties of Semiconducting Polymers. *Advanced Materials n/a* (n/a), 2313863. DOI: https://doi.org/10.1002/adma.202313863.
(12) Liang, Z.; Choi, H. H.; Luo, X.; Liu, T.; Abtahi, A.; Ramasamy, U. S.; Hitron, J. A.; Baustert, K. N.; Hempel, J. L.; Boehm, A. M.; et al. n-type charge transport in heavily p-doped polymers. *Nature Materials* **2021**, *20* (4), 518-524. DOI: 10.1038/s41563-020-00859-3 (acccessed 2023-08-24 00:36:12).www-nature-com.ezproxy.uky.edu.
(13) Xu, K.; Ruoko, T.-P.; Shokrani, M.; Scheunemann, D.; Abdalla, H.; Sun, H.; Yang, C.-Y.; Puttisong, Y.; Kolhe, N. B.; Figueroa, J. S. M.; et al. On the Origin of Seebeck Coefficient Inversion in Highly Doped Conducting Polymers. *Advanced Functional Materials* **2022**, *32* (20), 2112276. DOI: 10.1002/adfm.202112276 (acccessed 2022-05-18 13:36:54).Wiley Online Library.
(14) Joo, J. Charge transport of the mesoscopic metallic state in partially crystalline polyanilines. *Physical review.* **1998**, *57* (16), 9567-9580.
(15) Geng, X.; Du, T.; Xu, C.; Liu, Y.; Deng, Y.; Geng, Y. Realizing p-Type and n-Type Doping of a Single Conjugated Polymer via Incorporation of a Thienoisatin-Terminated Quinoidal Unit. *Advanced Functional Materials* **2023**, *33* (28), 2300809. DOI: https://doi.org/10.1002/adfm.202300809.
(16) Lee, T. S.; Lee, S. B.; Choi, D.-Y.; Suh, E. H.; An, T. K.; Jeong, Y. J.; Jang, J.; Kim, Y.-H. Doping and Thermoelectric Behaviors of Donor-Acceptor Polymers with Extended Planar Backbone.

Macromolecular Research **2021**, *29* (12), 887-894. DOI: 10.1007/s13233-021-9099-z (acccessed 2024-04-22 23:58:55).Springer Link.
(17) Han, J.; Song, Y.; Chen, N.; Chiu, A.; McGuiggan, P. M.; Adams, N.; Thon, S. M.; Tovar, J. D.; Katz, H. E. A Dichlorinated Dithienylethene-Diketopyrrolopyrrole-Based Copolymer with Pronounced P–N Crossover: Evidence for Anionic Seebeck Contribution. *ACS Materials Letters* **2022**, *4* (6), 1139-1145. DOI: 10.1021/acsmaterialslett.2c00267.
(18) Aubry, T. J.; Axtell, J. C.; Basile, V. M.; Winchell, K. J.; Lindemuth, J. R.; Porter, T. M.; Liu, J.-Y.; Alexandrova, A. N.; Kubiak, C. P.; Tolbert, S. H.; et al. Dodecaborane-Based Dopants Designed to Shield Anion Electrostatics Lead to Increased Carrier Mobility in a Doped Conjugated Polymer. *Advanced Materials* **2019**, *31* (11), 1805647. DOI: 10.1002/adma.201805647 (acccessed 2024-04-19 13:28:17).Wiley Online Library.
(19) Dyaga, B.; Lemaire, A.; Guchait, S.; Zeng, H.; Schmaltz, B.; Brinkmann, M. Impact of the dopant location in the semi-crystalline structure of alternated donor–acceptor copolymers on the polarity switching p → n mechanism. *Journal of Materials Chemistry C* **2023**, *11* (47), 16554-16562. DOI: 10.1039/D3TC02416D (acccessed 2024-04-23 00:24:53).pubs-rsc-org.ezproxy.uky.edu.
(20) Zhou, Q.; Zhan, C.; Wang, W.; Li, C.; Dong, D.; Xiao, S. Polarity Switch and Conductivity Enhancement of a Thermoelectric D–A Copolymer Enabled by Molecular Weight Control. *ACS Applied Polymer Materials* **2024**, *6* (1), 277-286. DOI: 10.1021/acsapm.3c01935.
(21) Jacobs, I. E.; D'Avino, G.; Lemaur, V.; Lin, Y.; Huang, Y.; Chen, C.; Harrelson, T. F.; Wood, W.; Spalek, L. J.; Mustafa, T.; et al. Structural and Dynamic Disorder, Not Ionic Trapping, Controls Charge Transport in Highly Doped Conducting Polymers. *Journal of the American Chemical Society* **2022**, *144* (7), 3005-3019. DOI: 10.1021/jacs.1c10651 (acccessed 2024-04-19 13:19:20).ACS Publications.
(22) Laan, P. C.; Bobylev, E. O.; Geels, N. J.; Rothenberg, G.; Reek, J. N.; Yan, N. Noncovalent Grafting of Molecular Complexes to Solid Supports by Counterion Confinement. *The Journal of Physical Chemistry C* **2023**, *127* (50), 24129-24136.
(23) Baustert, K. N.; Abtahi, A.; Ayyash, A. N.; Graham, K. R. Impact of the anion on electrochemically doped regioregular and regiorandom poly(3-hexylthiophene). *Journal of Polymer Science* **2021**, *60* (3), 602-609. DOI: 10.1002/pol.20210699.
(24) Neusser, D.; Malacrida, C.; Kern, M.; Gross, Y. M.; van Slageren, J.; Ludwigs, S. High conductivities of disordered P3HT films by an electrochemical doping strategy. *Chemistry of Materials* **2020**, *32* (14), 6003-6013.
(25) Comin, M.; Fratini, S.; Blase, X.; D'Avino, G. Doping-Induced Dielectric Catastrophe Prompts Free-Carrier Release in Organic Semiconductors. *Advanced Materials* **2022**, *34* (2), 2105376. DOI: 10.1002/adma.202105376 (acccessed 2023-12-21 20:59:09).Wiley Online Library.
(26) Liang, Z.; Boland, M. J.; Butrouna, K.; Strachan, D. R.; Graham, K. R. Increased power factors of organic–inorganic nanocomposite thermoelectric materials and the role of energy filtering. *Journal of Materials Chemistry A* **2017**, *5* (30), 15891-15900. DOI: 10.1039/c7ta02307c.

Author Contributions

A.O.Y. prepared the majority of the films, carried out EPR, spectroelectrochemistry, thermoelectric testing, and wrote the initial draft and worked through the revisions. K.N.B assisted with EPR measurements and thermoelectric testing. C.D.P. assisted with film preparation and spectroelectrochemistry measurements. K.R.G. directed the project and assisted with writing and revising the manuscript.

Funding

A.O.Y., K.N.B., C.D.P. and K.R.G. acknowledge the National Science Foundation (DMR-2349830) for primary support of this work and the National Science Foundation under cooperative agreement No. 1849213 for the ultrasonic spray coater used in this work. This work was performed in part at the U.K. Center for Electron Microscopy, a member of the National Nanotechnology Coordinated Infrastructure (NNCI), which is supported by the National Science Foundation (NNCI-2025075).

TOC Figure